International journal of basic and applied research

www.pragatipublication.com

ISSN 2249-3352 (P) 2278-0505 (E)

Cosmos Impact Factor-5.86

The Cohesive Zone Model for Numerical Analysis of Steel-Concrete Composite Structure Push-Out Tests

P.Vijay Kumar [1],M.Shiva Koti Reddy [2,] J.Nithin [3],

Associate Professor[1,] Professor[2,]UG Students[3,]

Department of CIVIL,

BRILLIANT GRAMMAR SCHOOL EDUCATIONAL SOCIETY'S GROUP OF INSTITUTIONS-INTEGRATED CAMPUS Abdullapurmet (V), Hayath Nagar (M), R.R.Dt. Hyderabad.

Abstract

The Action Plan is "socially sustainable" if and only if both the "propensity" and the "reduction in the number of accidents" are high. Figure 5 is an example of a formalization of this rule that uses Mamdani's sum-product inference [28] to ensure monotonicity in the results [22]. The FIS generates a set of fuzzy outputs, one for each of the three dimensions of sustainability, based on the values currently being fed into it for the input variables (indicators).

Introduction

To assess the efficacy of the F-BEM, we compared it to the widely used AHP technique, which assesses many pollution-reduction plans in light of a single case study. A total of 38,950 people live in the municipality of Mira, which is located in the province of Venice (population density: 393,81 people per square kilometer). Goods and people traveling between Padova and Venice utilize the majority of the transportation infrastructure (roads and trains). Approximately twenty percent of commutes were taken by buses along the primary route linking the two cities at the time of the study. Since the public transportation system in Mira was inadequate, most people drove themselves to and from work or school (about 60% of all trips). approximately 10% of all trips were made by persons riding bikes or walking, with most of these trips occurring inside the city limits (approximately 30% of all trips).

Exploring Possibly More Effective Policies

The procedure of assessment included looking at three distinct sets of policies: A. New Form of Urban Transportation (UTS) 1. High travel density during mornings and nights necessitates a UTS connecting the major areas to the train station. Passengers above the age of 75 and those who have valid transit cards may ride for free. Buses were used to transport the group of 19 customers. Table 2 details other service features. Second, a different kind of Dial-a-Ride service. Customers arranged for this service by contacting the Operations Centre, providing pick-up and destination locations inside the city limits (such as bus stops and railway stations) and the time they want to leave or arrive. The terminal accepted reservations up to 24 hours before the bus was scheduled to depart. The service was provided by a bus (with seating for up to 19 passengers), and tickets were priced similarly to those on the UTS. Table 2 provides a summary of further features. EOPN, is an alternate even-numbered plate number. During the hours of 8:00 a.m. and 10:00 a.m. on Tuesdays and Thursdays, only cars with catalytic converters and even-numbered license plates are allowed on the road. During the week used in the study, traffic volumes decreased by 2.5% on average. The examination also revealed other distinctions between the options.

Mechanical Description of Discontinuous Deformation

Consider a discontinuous physical domain Ω as shown in Figure 1.The domain contains a cohesive crack, and the cohesive interfaces can be denoted by $\Gamma+ c$ and $\Gamma- c$. The prescribed tractions F are

International journal of basic and applied research

www.pragatipublication.com

ISSN 2249-3352 (P) 2278-0505 (E)

Cosmos Impact Factor-5.86

imposed on boundary ΓF and the prescribed displacement u on Γu. The stress field inside the domain, σ, is related to the external loading F and the tractions t + and t − along the discontinuity through the equilibrium equations [20]:

$$\begin{aligned}
\operatorname{div}\boldsymbol{\sigma} + \mathbf{f} &= 0 \quad (\text{in}\,\Omega),\\
\boldsymbol{\sigma}\cdot\mathbf{n} &= \mathbf{F} \quad (\text{on}\,\Gamma_F),\\
\mathbf{u} &= \bar{\mathbf{u}} \quad (\text{on}\,\Gamma_u),\\
\mathbf{t}^{+} = \boldsymbol{\sigma}\cdot\mathbf{n}^{+} &= \mathbf{t} \quad (\text{on}\,\Gamma_c^{+}),\\
\mathbf{t}^{-} = \boldsymbol{\sigma}\cdot\mathbf{n}^{-} &= -\mathbf{t} \quad (\text{on}\,\Gamma_c^{-}).
\end{aligned}$$

Here the traction t is a function of the relative displacement w between Γ+ c and Γ− c , that is, t = t(w). The domain surrounding the discontinuity is assumed to be elastic. We further assume small strains and displacementMathematical Problems in Engineering 3 condition. Thus, the constitutive law and geometric equation for the domain can be written as

$$\begin{aligned}
\boldsymbol{\sigma} &= \mathbf{C} : \boldsymbol{\varepsilon} \quad (\text{in}\,\Omega \setminus \Gamma_c),\\
\boldsymbol{\varepsilon} = \boldsymbol{\varepsilon}(\mathbf{u}) &= \frac{\left[\nabla\mathbf{u} + (\nabla\mathbf{u})^{T}\right]}{2} \quad (\text{in}\,\Omega \setminus \Gamma_c)
\end{aligned}$$

Cohesive Zone Model

Figure 2 depicts the usual push-out test setup, including the interfaces between the concrete slabs and the steel girder flanges, as well as the shear connections and the surrounding concrete. During a push-out test, a cohesive bonding stress arises between the concrete and steel. When the bonding resistance is greater than the longitudinal shear stress, no slide is predicted at the contact. Interface slippage occurs when loads and longitudinal shear stresses both surpass the bonding resistance. Crack initiation and propagation occur when normal stress exceeds the tensile strength of the interface, leading to uplift pressures on the shear connections. Here, we employ a cohesive zone model to characterize the link between the interface shear stress and slip displacement and between the normal stress and the tensile displacement in order to perform a continuous-discontinuous deformation analysis of a push-out test. To explain the connection between cohesive stress and cracks dis placement during material fracture, Dugdale suggested the cohesive zone model [22]. Yang et al. [[23–26]] used a criteria suggested by Wang and Suo to examine mode-I and mode-II fracture by developing a functional connection between cohesive stress and the relative displacement. Fiber reinforced polymers (FRP) and concrete bond interface mechanical performance has been analysed using cohesive zone models [27, 28]. Ling et al. [20, 29] examined progressive failure at the soil-structure interface using an augmented finite element based on a cohesive zone model. Mechanical characteristics of the bond interface, including modulus, strength, and toughness, may be inferred using the cohesive zone model [30], provided the appropriate parameters are used. Figure 3 illustrates the multiple broken line mode cohesive zone model used here. In this model, normal displacement (w) and slip displacement (u) are denoted by different symbols. The normal and shear stresses are denoted by and. Mode-I and mode-II fractures have peak stresses of 1 and 1, respectively.

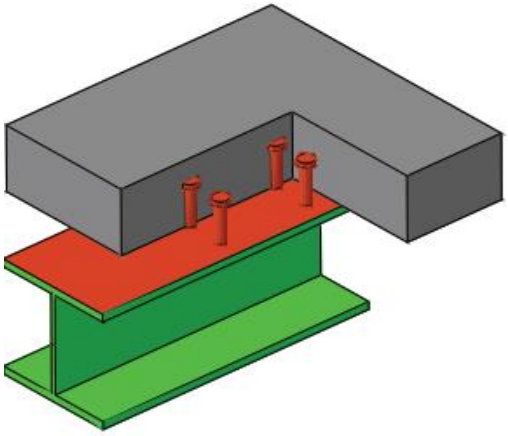

Figure 2: Interface between steel and concrete of typical push-out test.

The multiple broken lines mode cohesive zone model can be written as follows:

International journal of basic and applied research

www.pragatipublication.com

ISSN 2249-3352 (P) 2278-0505 (E)

Cosmos Impact Factor-5.86

$$\sigma = \begin{cases} K_n \Delta w, & (\Delta w \le 0), \\ \sigma_1, & (0 < \Delta w \le \Delta w_1), \\ \sigma_1 + \dfrac{\Delta w - \Delta w_1}{\Delta w_1 - \Delta w_2}(\sigma_1 - \sigma_2), & (\Delta w_1 < \Delta w \le \Delta w_2), \\ \sigma_2 + \dfrac{\Delta w - \Delta w_2}{\Delta w_2 - \Delta w_3}(\sigma_2 - \sigma_3), & (\Delta w_2 < \Delta w \le \Delta w_3), \\ 0, & \Delta w > \Delta w_3, \end{cases}$$

$$\tau = \begin{cases} \operatorname{sgn}(\Delta u)\,\tau_1, & (0 \le |\Delta u| \le \Delta u_1), \\ \operatorname{sgn}(\Delta u)\left[\tau_1 + \dfrac{|\Delta u| - \Delta u_1}{\Delta u_1 - \Delta u_2}(\tau_1 - \tau_2)\right], & (\Delta u_1 < |\Delta u| \le \Delta u_2), \\ \operatorname{sgn}(\Delta u)\,\tau_2, & |\Delta u| > \Delta u_2. \end{cases}$$

Cohesive Interface Element

A zero-thickness cohesive interface element was impleminted using a user-defined subroutine UEL in ABAQUS [21, 27, 31, 32]. In the user-defined element, the element stiffness matrix (AMATRX), nodal residual force vector (RHS), and state variables (SVARS) must be defined. The eight-node cohesive interface element used in this paper is shown in Figure 4. The nodal displacements of cohesive interface element in the global coordinate system are denoted by u; then, the relative displacement between the top and bottom nodes can be given as follows:

$$\boldsymbol{\delta}(\xi,\eta) = \sum_{i=1}^{4} \mathbf{N}_i(\xi,\eta)\left(\mathbf{u}_{i+4} - \mathbf{u}_i\right).$$

Here N(ξ, η) is the standard shape function. The matrix B(ξ, η) is defined as follows:

$$\mathbf{B} = \begin{pmatrix} -\mathbf{N}_1 & -\mathbf{N}_2 & -\mathbf{N}_3 & -\mathbf{N}_4 & \mathbf{N}_1 & \mathbf{N}_2 & \mathbf{N}_3 & \mathbf{N}_4 \end{pmatrix}.$$

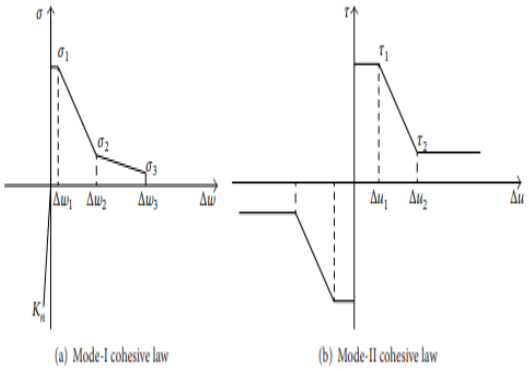

Figure 3: Cohesive zone model of interface.

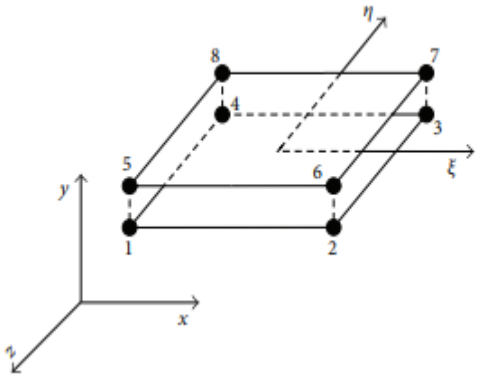

Figure 4: Cohesive interface element.

Finite Element Model of Push-Out Test

Testing for Push-Outs in Geometry.

This paper's analysis of a push-out test specimen had the same geometry as one employed in an experiment by Guezouli and Lachal [15]. Figure 6 depicts the push-out test specimen's geometric characteristics. The steel beam measured 260 mm in both height and breadth, with 17.5 mm flange plate and 10 mm web plate thicknesses. The dimensions of the concrete slab were 620 mm in length, 600 mm in breadth, and 150 mm in thickness. The transverse and longitudinal reinforcement in the concrete slab were 520 and 550 millimeters in length, respectively, with a 10 millimeter diameter. The studs were one centimeter in height. The stud heads were 31.7 mm in diameter, but the shanks were just 19 mm. 5.2.2.1 Material Specs. Figure 7(a) displays the constitutive relationship for the concrete employed in this study. The concrete slab has a Young's modulus of Ec = 36,900 MPa and a Poisson's ratio of 0.2. The model utilized the compression strength of a cylinder, fck = 56 MPa, and the tension strength, ft = 3.96 MPa. Literature data was used to determine that 0.8 fck = 44.8 MPa and 0.0012 strain were appropriate proportional limits [14, 17, 18]. The final compressive strain was 0.0022 times the strength at the point of failure. Concrete's ultimate strain at failure was 0.01 in compression and 0.005 in tension. The concrete component made use of an ABAQUS-based damage plasticity model. Steel beam, shear stud, and reinforcement all have the same Young's modulus of 210,000

International journal of basic and applied research

www.pragatipublication.com

ISSN 2249-3352 (P) 2278-0505 (E)

Cosmos Impact Factor-5.86

MPa. Steel has a Poisson's ratio of 0.3. For this analysis, an ideal elastic-plastic model was used to the steel beam. The steel beam's yield strength was 355 MPa. Figure 7(b) depicts the constitutive connection between the shear stud and the reinforcement. 500 MPa was the yield stress, while 550 MPa was the ultimate stress. Based on information available in the literature [10, 17, 33], strain before strain hardening and strain when ultimate stress is reached are set at 0.02 and 0.10, respectively.

Strain at strain hardening is set at 0.02, while strain at ultimate stress is set at 0.10, based on data from the literature [10, 17, 33].

Analysing Data Using Numbers

The bending and buckling resistance of the shear connector

Push-out test load-slip curves are shown in Figure 9(a).The ordinate value is the average force exerted by each stud, calculated by dividing the total action load by the total number of studs. The point U on Figure 6 represents the average slip at the interface's top, while the slip at the interface's base serves as the abscissa.

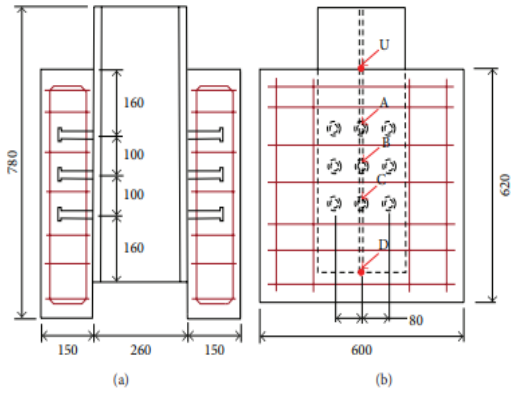

Figure 6: Push-out test model (unit: mm)

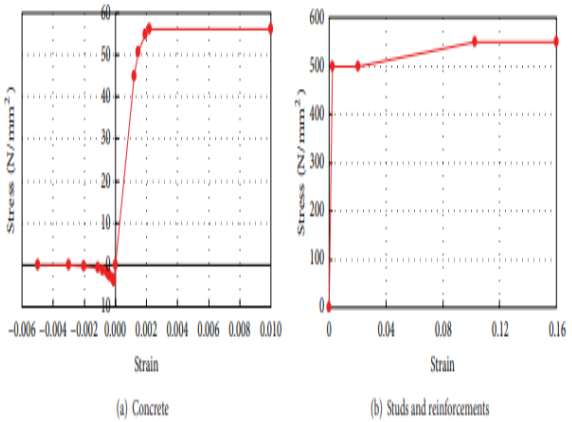

Figure 7: Constitutive laws for concrete, studs, and reinforcements

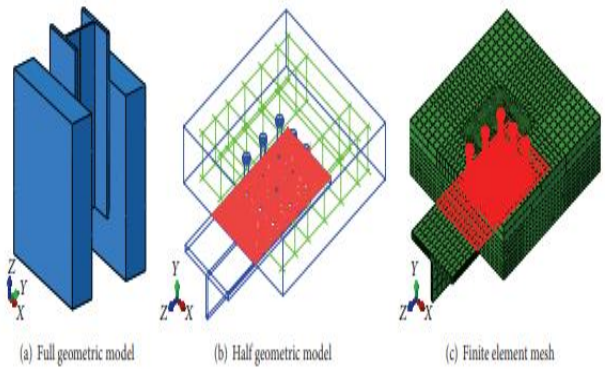

Figure 8: Finite element model.

of the interface (point D in Figure 6). The experimental results shown in Figure 9(a) were reported by Guezouli and Lachal [15]. Results of the shear strength of shear connectors calculated by Eurocode-4 and AASHTO LRFD are also shown in Figure 9(a)[39, 40].

Conclusions

In this research, the tangent slip and normal crack at the interfaces of the concrete slab and the steel girder flange, as well as the shear connections and the surrounding concrete, were characterized using a multiple broken lines mode cohesive zone model. Using ABAQUS's user-defined element sub procedure UEL, a zero-thickness cohesive element

International journal of basic and applied research

www.pragatipublication.com

ISSN 2249-3352 (P) 2278-0505 (E)

Cosmos Impact Factor-5.86

was added to a finite element model. The push-out testing procedure, including the load-displacement curve, relative displacement of the interfaces, and stress distribution at the interfaces, was modelled using three-dimensional numerical analysis. The research has led to the following inferences. (1) The method proposed in this paper is able to precisely determine (a) the shear strength and shear stiffness of the shear connectors, (b) the normal separation and tangential slip of the interfaces between the concrete slab and the steel girder flange, and (c) the normal separation and tangential slop of the interfaces between the shear connectors and the surrounding concrete. Even at light loads, there was separation between the stud root and the concrete on the surface perpendicular to the load. Separation values for the push-out test model used in this article were highest at the top stud and lowest at the center stud. The findings revealed a non-uniform distribution of normal separation and tangential slip at the interface of the concrete slab and the steel girder flange.

References

[1] L. An and K. Cederwall, "Push-out tests on studs in high strength and normal strength concrete," Journal of Constructional Steel Research, vol. 36, no. 1, pp. 15–29, 1996.

[2] J. C. Chapman and S. Balakrishnan, "Experiments on composite beams," Structural Engineer, vol. 42, no. 11, pp. 369–383, 1964.

[3] B. S. Jayas and M. U. Hosain, "Behaviour of headed studs in composite beams: push-out tests," Canadian Journal of Civil Engineering, vol. 15, no. 2, pp. 240–253, 1988.

[4] R. P. Johnson and D. J. Oehlers, "Analysis and design for longitudinal shear in composite T-beams," in Proceedings of the Institution of Civil Engineers, pp. 989–1021, 1981.

[5] J. G. Ollgaard, R. G. Slutter, and J. W. Fisher, "Shear strength of stud connectors in lightweight and normalweight concrete," Engineering Journal, vol. 8, no. 2, pp. 55–64, 1971. [6] L. Pallares and J. F. Hajjar, "Headed steel stud anchors in composite structures I: Shear," Journal of Constructional Steel Research, vol. 66, no. 2, pp. 198–212, 2010.

[7] D. Xue, Y. Liu, Z. Yu, and J. He, "Static behavior of multi-stud shear connectors for steel-concrete composite bridge," Journal of Constructional Steel Research, vol. 74, pp. 1–7, 2012.

[8] E. C. Oguejiofor and M. U. Hosain, "Numerical analysis of pushout specimens with perfobond rib connectors," Computers and Structures, vol. 62, no. 4, pp. 617–624, 1997.

[9] S. Al-Darzi, A. R. Chen, and Y. Q. Liu, "Parametric studies of push-out test with perfobond rib connector," in Proceedings of China-Japan Joint Seminar on Steel and Composite Bridges, pp. 103–111, 2007.

[10] O. Mirza and B. Uy, "Effects of the combination of axial and shear loading on the behaviour of headed stud steel anchors," Engineering Structures, vol. 32, no. 1, pp. 93–105, 2010.

[11] C. Kalfas and P. Pavlidis, "Load-slip curve of shear connectors evaluated by FEM analysis," in Proceedings of the International Conference, Composite Construction-Conventional and Innovative, pp. 151–156, Innsbruck, Austria, 1997.

[12] B. Kim, H. D.Wright, and R. Cairns, "The behaviour of throughdeck welded shear connectors: an experimental and numerical study," Journal of Constructional Steel Research, vol. 57, no. 12, pp. 1359–1380, 2001.

[13] D. Lam and E. El-Lobody, "Behavior of headed stud shear connectors in composite beam," Journal of Structural Engineering, vol. 131, no. 1, pp. 96–107, 2005.

[14] E. Ellobody and B. Young, "Performance of shear connection in composite beams with profiled

steel sheeting," Journal of Constructional Steel Research, vol. 62, no. 7, pp. 682–694, 2006.

[15] S. Guezouli and A. Lachal, "Numerical analysis of frictional contact effects in push-out tests," Engineering Structures, vol. 40, pp. 39–50, 2012.

[16] C. Xu, K. Sugiura, C. Wu, and Q. Su, "Parametrical static analysis on group studs with typical push-out tests," Journal of Constructional Steel Research, vol. 72, pp. 84–96, 2012

. [17] J. Okada, T. Yoda, and J. Lebet, "A study of the grouped arrangements of stud connectors on shear strength behavior," Structural Engineering/Earthquake Engineering, vol. 23, no. 1, pp. 75s–89s, 2006.

[18] H. T. Nguyen and S. E. Kim, "Finite element modeling of push-out tests for large stud shear connectors," Journal of

Constructional Steel Research, vol. 65, no. 10-11, pp. 1909–1920, 2009.

[19] ABAQUS, User's Manual 6.10, Dassault Systemes Simulia, Prov- ` idence, RI, USA, 2010.

[20] D. Ling, Q. Yang, and B. Cox, "An augmented finite element method for modeling arbitrary discontinuities in composite materials," International Journal of Fracture, vol. 156, no. 1, pp. 53–73, 2009.

[21] N. Moes and T. Belytschko, "Extended finite element method for ¨ cohesive crack growth," Engineering Fracture Mechanics, vol. 69, no. 7, pp. 813–833, 2002. [22] D. S. Dugdale, "Yielding of steel sheets containing slits," Journal of the Mechanics and Physics of Solids, vol. 8, no. 2, pp. 100–104, 1960